ARTICLE

Bulk crystal growth and characterization of non-centrosymmetric single crystal $CaTa_4O_{11}$

Received 00th January 20xx,
Accepted 00th January 20xx

DOI: 10.1039/x0xx00000x

Yueshen Zhou,[ab] Dongsheng Yuan*[a] and Kiyoshi Shimamura*[ab]

Bulk single crystals of non-centrosymmetric $CaTa_4O_{11}$ were grown successfully by the floating-zone method for the first time, despite that the already reported CaO-Ta_2O_5 phase diagram indicates its incongruent melting behavior. The as-grown crystal rods (Φ 5-6 mm) have a black and a colorless transparent appearance grown in Ar and O_2 atmospheres, respectively. Subsequently, O_2 atmosphere was selected to optimize its bulk crystal growth. The $CaTa_4O_{11}$ single crystals show a good crystallinity with the evidence of a symmetric X-ray rocking curve for 004 diffraction with a FWHM of 72'', although the fabrication technique has the drawback of an extremely high thermal gradient for crystal growth. For this new hexagonal bulk single crystal, its anisotropic optical, dielectric, and thermal properties were characterized. The crystal has a transmittance of ~78% from the cut-off edge 350 nm till 800 nm. When excited by both 254 nm UV and X-ray, it shows a broad band emission with a peak wavelength around 427 nm. The dielectric constants ε_{11} and ε_{33} were found to be 30 and 52.3, respectively at 1 kHz. Meanwhile, the thermal conductivity along the *c*-axis is 5.69 $Wm^{-1}K^{-1}$, which is 1.8 times higher than that along the *a*-axis, which measures 3.19 $Wm^{-1}K^{-1}$ at room temperature.

Introduction

Single crystals of tantalates have garnered great attention across virous applications including nonlinear optics, scintillation, piezoelectricity/pyroelectricity, etc [1-4]. Among these, several single-crystal alkaline-earth tantalates have been grown by the conventional melting techniques such as Czochralski, Bridgman and floating-zone methods to explore their properties and applications. For instance, MTa_2O_6 (where M represents Mg, Ca, and Sr) crystals were studied as laser active media and microwave resonators [5-8]. The acoustic response of $Sr_2Ta_2O_7$ single crystals was investigated for employment in ferroelectric random-access memories [9]. As potential scintillators for high-energy X-ray radiography, $Mg_4Ta_2O_9$ single crystals were found to show bright intrinsic radioluminescence, promoting alkaline-earth tantalates as promising intrinsic scintillator candidates [10,11].

The CaO-Ta_2O_5 system was reported by K. T. Jacob et al. to have four stoichiometric compounds: $CaTa_4O_{11}$, $CaTa_2O_6$, $Ca_2Ta_2O_7$, and $Ca_4Ta_2O_9$ [12]. To explore functional properties in this family, their single crystals in bulk form are highly demanded. Despite this binary phase diagram was already established via the synthesis method of high-temperature solid-solid reaction as reproduced in Fig. 1 [13], the melting behaviours of the stoichiometric compounds were still pending questions until their melting-growth study.

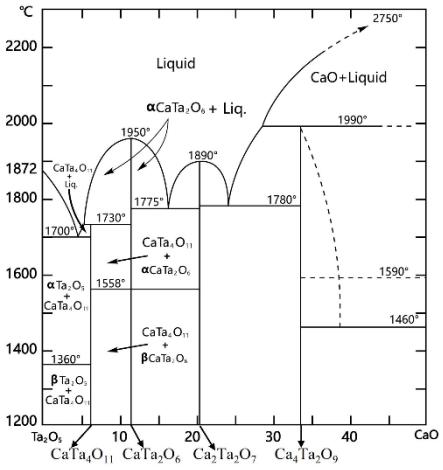

Fig. 1. The reported CaO-Ta_2O_5 phase diagram above 1200 °C [13].

$CaTa_2O_6$ and $Ca_2Ta_2O_7$ were observed to show polymorphs: orthorhombic & tetragonal & cubic structures for the former and trigonal & monoclinic for the latter, thus their crystal growths require quenching to avoid the corresponding phase transitions [14,15]. C. R. Ferrari et al. used the laser-heated pedestal growth (LHPG) method that can achieve rapid cooling but can only obtain thin and small samples in a diameter of ~700 μm, not to mention bulk single crystals over 5 mm in size [6]. Regarding $CaTa_4O_{11}$ and $Ca_4Ta_2O_9$, the phase diagram indicates their incongruent melting behaviors. To the best of our knowledge, there has been no report of single-crystal form of $Ca_4Ta_2O_9$. What interests us is the Ta-richest compound here, $CaTa_4O_{11}$, which shows a great potential as a scintillator due to its high density (7.57 g/cm^3) and effective atomic number (68.4).

[a] National Institute for Materials Science, Tsukuba 305-0044, Japan. Email: YUAN.dongsheng@nims.go.jp, SHIMAMURA.Kiyoshi@nims.go.jp
[b] Graduate School of Advanced Science and Engineering, Waseda University, Shinjuku, Tokyo 169-8555, Japan.

Although Akashi et al. mentioned the synthesis of crystal samples using the floating-zone technique in 1969 [16], however, no subsequent reports on either bulk single crystal growth or the basic physical properties of $CaTa_4O_{11}$ were seen. To answer the question that $CaTa_4O_{11}$ melts incongruently as reported in the phase-diagram [13] or not and further investigate potential properties of $CaTa_4O_{11}$ single crystals, we studied its crystal growth using the Xenon lamp floating zone method.

In this work, $CaTa_4O_{11}$ bulk single crystal growth in different atmospheres were investigated. The optimized high-quality crystal was characterized in terms of structural, anisotropic optical, thermal, and dielectric properties.

Experimental

Crystal growth

Polycrystalline $CaTa_4O_{11}$ rods were fabricated through the traditional solid-state reaction method using high-purity (99.99%) Ta_2O_5 and $CaCO_3$ raw materials. Initially, the stoichiometric powders of raw materials were weighed and mixed thoroughly. A follow-up calcination was carried out at 1100 °C for 10 hours in air. After calcination, the powders were packed into a rubber tube and then pressed isostatically under 300 MPa. The pressed rods were subsequently sintered in air at 1300 °C for 10 hours, resulting in the production of dense ceramic rods.

Single-crystal growth of $CaTa_4O_{11}$ was conducted using a Xenon lamp floating-zone furnace. The growth rate was 6 mm/h. During the growth process, the feed rod rotated at a speed of 26 rpm, while the seed rod at 13 rpm in the opposite direction. Both argon (Ar) and oxygen (O_2) atmospheres were employed to optimize the crystal quality.

Characterization

The powder X-ray diffraction analysis was conducted by a Rigaku SmartLab3 diffractometer (Cu Kα X-ray radiation with a wavelength of 1.54059 Å). The crystal quality was evaluated by X-ray rocking curve measurement on a *c*-oriented sample, using a high-resolution X-ray diffractometer of PANalytical X'Pert PRO. Optical transmittance were measured with a JASCO spectrometer V-570. Photoluminescence (PL) spectrum was acquired using a JASCO FP-8650FDA fluorescence spectrometer. An X-ray generator was used for measuring the X-ray excited luminescence spectrum [17]. Dielectric constants were determined at a frequency of 1 kHz utilizing an LCR meter (Hioki IM3536). The Dulong-Petit law was applied to estimate the specific heat capacity (C_p) [18], while thermal diffusivity measurements were carried out through a laser flash method using an LFA 467 instrument from NETZSCH.

Results and discussion

Crystals and Structure

Figure 2 shows the images of single-crystal $CaTa_4O_{11}$ grown in Ar and O_2 atmosphere. $CaTa_4O_{11}$ crystal grown in Ar presents a black color as shown in Fig. 2(a). This originates from the reduction of Ta^{5+} to Ta^{4+} at high temperature in an oxygen-deficient atmosphere and correspondingly the formation of oxygen vacancies [5]. Conversely, growing the crystal in an O_2 atmosphere effectively eliminates the black color, resulting in a colorless and transparent single crystal, as shown in Fig. 2(b). Powder X-ray diffraction analysis confirmed that the as-grown crystals are single-phase hexagonal, with profiles matching the ICSD reference (01-070-0847), as illustrated in Fig. 3 [16].

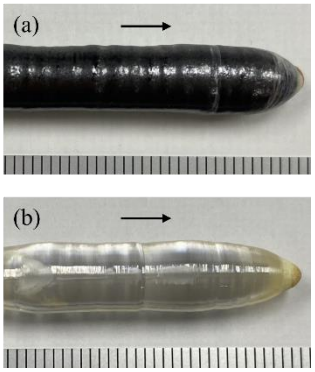

Fig. 2. Images of the $CaTa_4O_{11}$ crystals grown from (a) Ar and (b) O_2. The black arrows show the direction of the crystal growth.

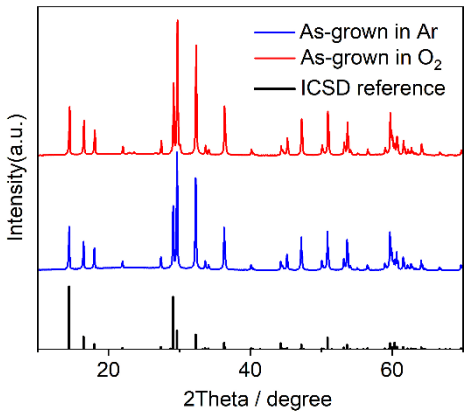

Fig. 3. Powder X-ray diffraction patterns of the as-grown single-crystal $CaTa_4O_{11}$.

The X-ray rocking curve of 004 diffraction peak is shown in Fig. 4. The curve is symmetric and has a full width at half maximum (FWHM) of 72″, indicating a good crystallinity of the as-grown crystals.

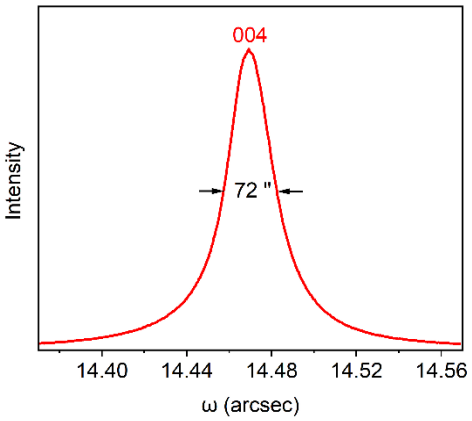

Fig. 4. X-ray rocking curve of O_2-grown $CaTa_4O_{11}$ crystal.

Given the absence of reliable crystal structure reports from high-quality $CaTa_4O_{11}$ bulk single crystals, here the crystal structure was analyzed. The structure and refinement data of $CaTa_4O_{11}$ are listed in Table 1 with a more reasonable R-factor than all reported values [16, 19]. The corresponding cif file is given in the ESI‡. $CaTa_4O_{11}$ crystallizes in the hexagonal system with the space group of $P6_322$ ($a = b = 6.2127$ Å, $c = 12.2638$ Å). Fig. 5(a) shows an asymmetric unit and the corresponding bonding lengths of $CaTa_4O_{11}$. One of the Ta atoms, designated as Ta2, is coordinated by seven oxygen atoms, forming a pentagonal bipyramid. The remaining Ta (Ta1) and Ca atoms are surrounded by six and eight oxygen atoms, respectively. Fig. 5(b) shows the crystal structure of $CaTa_4O_{11}$ single crystal projected to <110> direction. We can see that it contains an alternant structure with a layer formed by Ta2 pentagonal bipyramids and another layer formed by Ta1 and Ca atoms where both layers are parallel to the *c*-plane.

Table 1 Crystal data and structure refinement of $CaTa_4O_{11}$ single crystal

Empirical formula	$CaTa_4O_{11}$
Formula weights (g mol^{-1})	939.88
Temperature (K)	297
Crystal system, space group	Hexagonal, $P6_322$
Unit cell dimensions (Å)	a=b=6.2127 (2), c=12.2638(4)
V (Å^3)	409.94 (3)
Density (g cm^{-3})	7.614
Z	2
F_{000}	800
Absorption coefficient (mm^{-1})	53.885
Theta range (deg.)	3.753-29.169
Limiting indices	$-8 \le h \le 7$, $-6 \le k \le 8$, $-15 \le l \le 15$
Reflection number	5531
Unique/collected reflection number	355/349
R_{int}	0.0402
Final R indices [$I > 2\sigma(I)$]	0.0134/0.0299
R indices (all data)	0.0141/0.03
Goodness-of-fit	1.276
Largest diff. peak and hole (e/Å^3)	0.942/-0.931

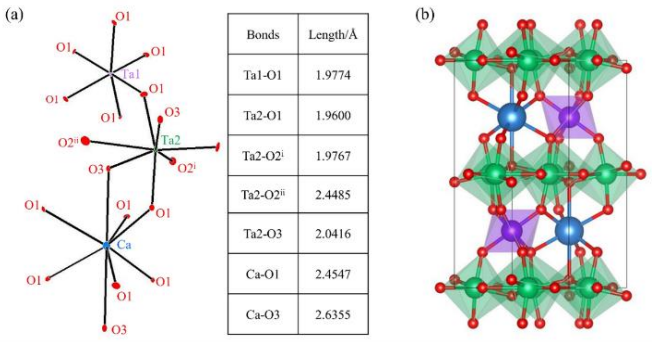

Bonds	Length/Å
Ta1-O1	1.9774
Ta2-O1	1.9600
Ta2-O2^i	1.9767
Ta2-O2^{ii}	2.4485
Ta2-O3	2.0416
Ca-O1	2.4547
Ca-O3	2.6355

Fig. 5 (a) An asymmetric unit formed by one TaO6 group, one TaO7 group, and the Ca atom in eightfold oxygen coordination, together with their corresponding interatomic distances, (b) crystal structure of $CaTa_4O_{11}$ single crystal projected to <110> direction.

Optical and luminescence properties

The transmission spectra of $CaTa_4O_{11}$ single crystals obtained in an O_2 atmosphere for the (010) and (001) planes are displayed in Fig. 6(a). Both exhibit a transmittance of approximately 78% across the wavelength range from 350 to 800 nm. To determine its optical band gap, the Tauc formula $(\alpha h\nu)^{1/n} = A^{1/n}(h\nu - E_g)$ was applied, and a better fitting was achieved with n = 1/2, as illustrated in Fig. 6(b) [20]. This finding suggests that it has a direct band gap of about 4.5 eV. Fig. 6(c) presents the excitation and emission spectra where a dominant excitation band appears at 255 nm and the corresponding emission band shows a peak wavelength at 427. It can be seen in the fitted emission spectrum that the dominant emission broad band was deconvoluted into only one peak as shown in Fig. S1‡. According to the previous research, this might originate from the Ta-O charge-transfer transition associated with the TaO_6/TaO_7 polyhedrons in $CaTa_4O_{11}$ [21]. Under X-ray excitation, $CaTa_4O_{11}$ also exhibits a band with a peak wavelength around 427 nm, as depicted in Fig. 6(d). The similarity of the spectrum to the PL one implies the same emission center for both UV and X-ray excitation.

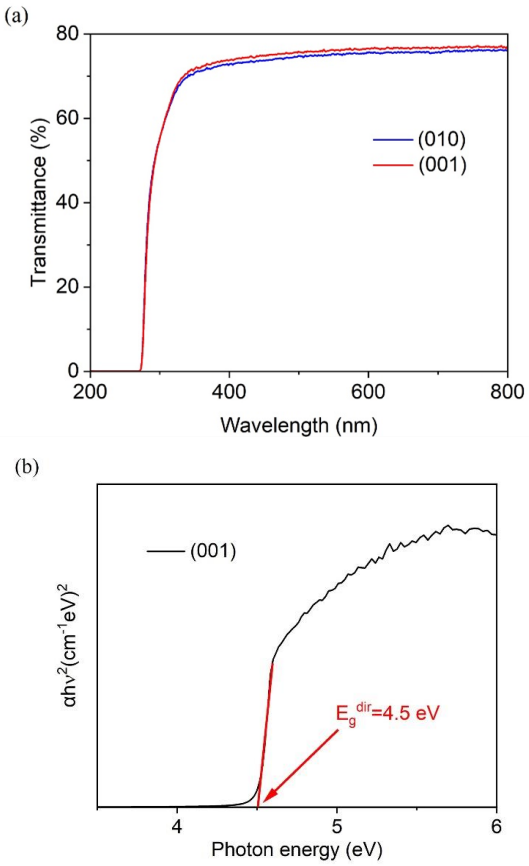

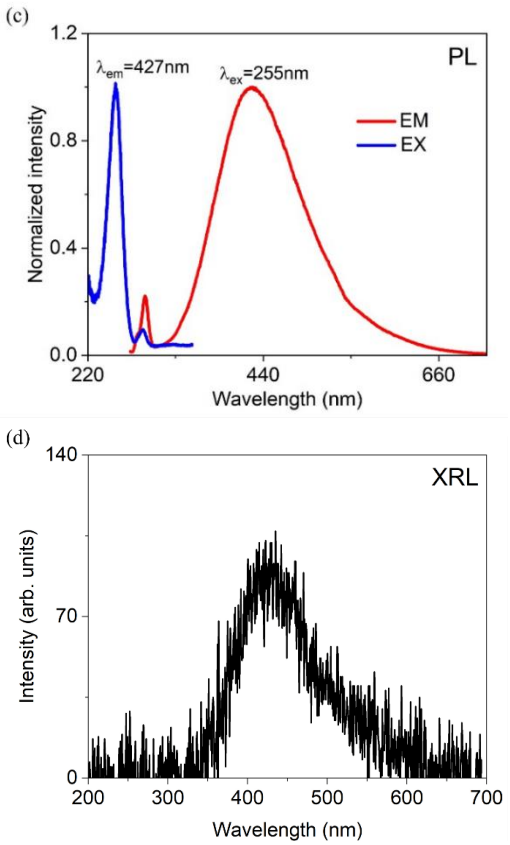

Fig. 6. (a) Transmission spectra of $CaTa_4O_{11}$, (b) the variation of $(\alpha h\nu)^2$ vs. photon energy ($h\nu$), (c) PL excitation and emission spectra of $CaTa_4O_{11}$, (d) X-ray luminescence spectrum.

Dielectric constants

$CaTa_4O_{11}$ has two independent dielectric constants and were measured at 1kHz as $\varepsilon_{11} = 30$ and $\varepsilon_{33} = 52.3$. Table 2 lists the dielectric constants of $CaTa_4O_{11}$ crystal, in comparison with α-quartz, and some other tantalates crystals. The dielectric constant ε_{33} of $CaTa_4O_{11}$ is larger than those of α-quartz, $Ca_3TaGa_3Si_2O_{14}$, and $LiTaO_3$, but lower than that of $SrTa_2O_6$.

Table 2 Dielectric constants of $CaTa_4O_{11}$ crystal in comparison with α-quartz, $Ca_3TaGa_3Si_2O_{14}$, $LiTaO_3$ and $SrTa_2O_6$ crystals

Crystal	ε_{11}	ε_{33}
$CaTa_4O_{11}$	30	52.3
α-quartz [22]	4.5	4.6
$Ca_3TaGa_3Si_2O_{14}$ [23]	16.3	21.6
$LiTaO_3$ [24]	54	43
$SrTa_2O_6$ [8]	108	128

Thermal conductivity

The thermal conductivity can be calculated by the equation: $k = \lambda\rho C_p$, where k, λ, ρ and C_p denote the thermal conductivity, thermal diffusivity coefficient, density, and specific heat capacity of the crystal, respectively [25]. The thermal conductivity k_{ij} of a crystal is also a symmetrical second-rank tensor like the electric permittivity, and for point group 622, the matrix controlled by Neumann's principle is the following form [26, 27]:

$$k_{ij} = \begin{matrix} k_{11} & 0 & 0 \\ 0 & k_{11} & 0 \\ 0 & 0 & k_{33} \end{matrix}$$

So, the thermal diffusivity coefficients of the $CaTa_4O_{11}$ crystal were measured along the *a*-axis and *c*-axis by a laser flash method, and the results are shown in Fig. 7(a). The specific heat capacity was estimated by the Dulong-petit law, utilizing the equation $C_p = 3rR/M$, where r = 16 is the number of atoms in one formula, with the gas constant R being 8.314 J/(k·mol), and M for molar mass being 939.86 g/mol. The calculated C_p is approximately 0.42 J/(k·g). Note that the Dulong-petit law is not a sufficiently accurate measure, and the calculated C_p value might be a little bit higher than the real ones [18]. From the Fig. 7(b), we can see that as the temperature rises, the thermal conductivity of the $CaTa_4O_{11}$ crystal decreases. This phenomenon can be attributed to heightened phonon scattering due to vigorous atomic vibrations and the increased average interatomic distance resulting from lattice expansion. The thermal conductivity anisotropy, with a higher value along the *c*-axis, can be attributed to the alternant layer structure along this axis which promotes stronger atomic bonding and consequently increases thermal conductivity [28].

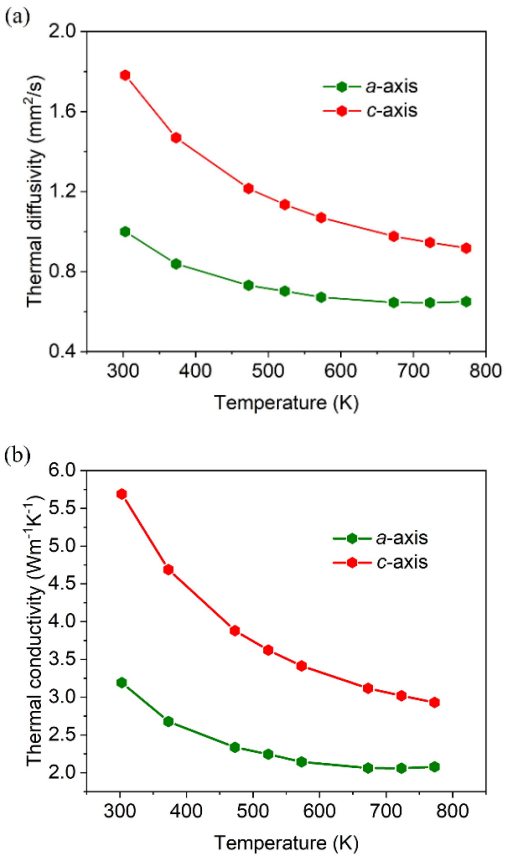

Fig. 7. Temperature dependence of the (a) thermal diffusivity, (b) thermal conductivity of single crystal $CaTa_4O_{11}$.

Conclusions

For the first time, high-quality bulk single crystals of $CaTa_4O_{11}$ were grown by the floating-zone method, and thus the current phase-diagram was revised for the stoichiometry $CaO{\cdot}2Ta_2O_5$, showing a congruently melting behavior. The crystal became black in an Ar atmosphere due to oxygen vacancies and recovered to the intrinsic colourless when grown in an O_2 atmosphere. Its crystallographic quality was characterized with a FWHM of 72'' in XRC. The O_2-grown crystals has a transmittance of approximately 78% and a broad band emission centered around 427 nm when excited under UV and X-ray. Given its high stopping power of X- and γ-ray, this single crystal holds promise as a potential host for scintillation applications when it is properly activated. The dielectric constants ε_{11} and ε_{33} are 30 and 52.3, respectively, at 1 kHz. Additionally, the thermal conductivity along the *c*-axis is 1.8 times higher than along the *a*-axis, measuring 5.69 $Wm^{-1}K^{-1}$ and 3.19 $Wm^{-1}K^{-1}$ at room temperature, respectively.

Conflicts of interest

There are no conflicts to declare.

Acknowledgements

The authors would like to sincerely thank Mr. Satoshi Yamamoto for his kind support with crystal polishing and Dr. Yoshitaka Matsushita for his support of crystal structure analysis. This work was supported by "Advanced Research Infrastructure for Materials and Nanotechnology in Japan (ARIM)" of the Ministry of Education, Culture, Sports, Science and Technology (MEXT). Proposal Number JPMXP1223NM5337.

Notes and References

‡ Electronic supplementary information.

[1] A. Hossain and M. H. Rashid, IEEE Trans. Ind. Appl. 1991, 27, 824–829.
[2] J. G. Gualtieri, J. A. Kosinski, and A. Ballato, IEEE Trans. Ultrason. Ferroelectr. Freq. Control. 1994, 41, 53–59.
[3] R. Dou, Q. Zhang, J. Gao, Y. Chen, S. Ding, F. Peng, W. Liu and D. Sun, Crystals, 2018, 8, 1-21.
[4] E. D. Bourret, D. M. Smiadak, R. B. Borade, Y. Ma, G. Bizarri, M. J. Weber and S. E. Derenzo, J. Lumin., 2018, 202, 332-338.
[5] M. Higuchi, K. Ando, J. Takahashi and K. Kodaira, JCS-Japan, 1993, 101, 118-120.
[6] C. R. Ferrari, A. S. S. de Camargo, L. A. O. Nunes and A. C. Hernandes, J. Cryst. Growth, 2004, 266, 475-480.
[7] A. S. S. de Camargo, C. R. Ferrari, A. C. Hernandes and L. A. O. Nunes, J. Phy Condens. Matter, 2004, 16, 5915-5923.
[8] I. Tanaka, Y. Sato and H. Kojima, J. Cryst. Growth, 1990, 99, 837-840.
[9] A. Hushur and S. Kojima, Mater. Sci. Eng. A, 2006, 442, 35-38.
[10] D. Yuan, F. Moretti, D. Perrodin, G. Bizarri, T. Shalapska, C. Dujardin and E. Bourret, CrystEngComm, 2022, 22, 3497-3504.
[11] T. Hayashi, K. Ichiba, D. Nakauchi, K. Watanabe, T. Kato, N. Kawaguchi and T. Yanagida, J. Lumin, 2023, 255. 119614.
[12] K. T. Jacob and A. Rajput, J. alloys Compd, 2015, 620, 256-262.
[13] D. A. Reeve, J. Less-Common Met, 1969, 17, 215-222.
[14] N. G. Teixeira, R. L. Moreira, R. P. S. M. Lobo, M. R. B. Andreeta, A. C. Hernandes and A. Dias, Cryst. Growth Des., 2011, 11, 5567-5573.
[15] I. E. Grey, R. S. Roth, W. G. Mumme, J. Planes, L. Bendersky, C. Li and J. Chenavas, J. Solid State Chem, 2001, 161, 274-287.
[16] M. Isobe, F. Marumo and S. Iwai, Acta Cryst., 1975, B31, 908-910.
[17] T. Yanagida, M. Koshimizu, G. Okada, T. Kojima, J. Osada and N. Kawaguchi, Opt. Mater., 2016, 61, 119-124.
[18] S. Tanusilp, Y. Ohishi, H. Muta, S. Yamanaka, A. Nishide, J. Hayakawa and K. Kurosaki, Phys. Status Solidi PRL, 2017, 12, 1700372.
[19] L. Jahnberg, J. Solid State Chem., 1970, 1, 454-462.
[20] P. Makula, M. Pacia and W. Macyk, J. Phys. Chem. Lett., 2018, 9, 6814-6817.
[21] L. Qin, D. Wei, Y. Huang, S. I. Kim, Y. M. Yu and H. J. Seo, Inorg. Chem., 2013, 52, 10407-10413.
[22] W. Dong, Y. Sun, B. Wang, M. Zhu, J. Li, X. Xu and J. Wang, Cryst. Growth Des. 2022, 22, 4243−4249.
[23] X. Fu, E. G. Villora, Y. Matsushita, Y. Kitanaka, Y. Noguchi, M. Miyayama, K. Shimamura and N. Ohashi, RSC Adv., 2017, 7, 56697-56703.
[24] Roditi International, Lithium Tantalate, https://roditi.com/SingleCrystal/Lithium-Tantalate/$LiTaO_3$ Properties.html, (accessed June 2, 2024).
[25] W. Zhang, X. Tao, C. Zhang, and M. Jiang, Cryst. Growth Des. 2009, 9, 2633-2636.
[26] R. E. Newnham, 'Tensors and physical properties', Properties of Materials: Anisotropy, Symmetry, Structure (Oxford, 2004; online edn, Oxford Academic, 12 Nov. 2020).
[27] R. Mckinney, P. Gorai, E. Toberer and V. Stevanovic, Chem. Mater., 2020, 32, 3320-3321.
[28] S. Mukhopadhyay, L. kindsay and D. J. Singh, Sci. Rep., 2016, 6, 37076.